PCCP

PAPER

View Article Online
View Journal | View Issue



Cite this: *Phys. Chem. Chem. Phys.*, 2014, **16**, 11390

# Effect of stepped substrates on the interfacial adhesion properties of graphene membranes

Yan He, Wangbing Yu and Gang Ouyang*

Received 12th February 2014,
Accepted 20th March 2014

DOI: 10.1039/c4cp00633j

www.rsc.org/pccp

In order to gain a comprehensive understanding of interface adhesion properties involved in adhesion energy and local interface separation between graphene membranes and underlying stepped substrates, we develop an analytic model by considering the total free energy originally from interfacial van der Waals interaction and elastic strain energy stored in the membranes based on an atomic-bond-relaxation consideration. It is found that the interface adhesion energy decreases with increasing membrane thickness. Moreover, as compared to the case of a flat substrate surface, the interface adhesion properties of graphene membranes on stepped surfaces are strongly affected by the substrate surface parameters, including step height, vicinal angle, membrane thickness, terrace width and orientation, *etc.*, implying that the topographic fluctuation of graphene is attributed to the various interface separations at different substrate sites. Our predictions agree reasonably well with computer simulations and experimental observations, which suggest that the developed method can be regarded as an effective method to design the interface adhesion of graphene membranes in graphene-based functional device components.

## Introduction

In recent years, graphene has become one of the focused problems in physics, chemistry and material science due to its charming properties and wide range of potential applications.[1,2] Conventionally, researchers prepared the high-quality graphene on various substrates such as metals and semiconductors in order to explore its exceptional performances.[3–5] Therefore, the interfacial properties between graphene and its substrate contacts are very important and should be clarified in detail. So far, many investigations have been made to pursue the interfacial properties including adhesion energy and interface separation from the aspects of experiment measurements and theoretical calculations.[3,6–9]

In general, the physical properties of graphene are strongly affected by the underlying substrate.[10–12] Recent work by Koenig *et al.*[3] experimentally measured that the interfacial adhesion energies between graphene and $SiO_2$ are $0.45 \pm 0.02$ J m$^{-2}$ to $0.31 \pm 0.03$ J m$^{-2}$ for the monolayer to multilayers with 2–5 layers. Yoon *et al.*[4] reported the adhesion energy between graphene and Cu is $0.72 \pm 0.07$ J m$^{-2}$. Theoretically, Neek-Amal *et al.*[9] found the interfacial bond strength and the distribution of membrane strain are influenced by the morphology of the substrate surface (*e.g.*, a corrugated surface). Also, some other factors involved in substrate roughness, membrane thickness and surface forces have been taken into account in the interfacial interaction of graphene and related systems. In particular, a kind of peculiar morphology such as sinusoid corrugation has also considered both experimentally and theoretically. For instance, Scharfenberg *et al.*[13,14] demonstrated the substrate morphology and membrane thickness have an effect on the interfacial adhesion energy in graphene systems. Gao *et al.*[15] predicted the interfacial adhesion energy can be related with the substrate roughness and amplitude. Moreover, they suggested that the van der Waals interaction between graphene and its substrate and the bending strain energy of graphene play the important roles for the adjustment of equilibrium graphene conformation. As a result, it is concluded that not only various types of substrates but also surface morphologies of substrates have significant effects on the interfacial adhesion properties.

However, the real morphology of the substrate surface cannot usually be approached as an ideal flat surface or any other regular period figure. For example, the real surface of substrates is rough and possesses many terraces and steps. A large number of un-flat or stepped substrate surfaces have been detected in experiments such as Cu,[16] Ir,[17] Ni,[18,19] SiC,[20,21] $SiO_2$ (ref. 22 and 23) and so on. Subsequently, the stepped substrate will make the upper epitaxial layer be very different from that of the idea flat case.[24–26] Although many efforts have been employed to explore the interface and related properties in graphene membranes, a systematic study to illustrate the adhesion energy and interface separation for graphene on stepped substrates from the atomistic origin is still lacking. Furthermore, the influences of surface relaxation and interfacial mismatch on the interfacial interaction between graphene and underlying substrate are unclear so far.

*Key Laboratory of Low-Dimensional Quantum Structures and Quantum Control of Ministry of Education and Department of Physics, Hunan Normal University, Changsha 410081, China. E-mail: gangouy@hunnu.edu.cn*

 

In order to explore the relationship between the interfacial adhesion between graphene and the underlying substrate, in this work we present an analytical method to explore the issue by taking into account the free energies induced by membrane thickness and substrate surface parameters including terrace width and step height, *etc.*, from the perspective of atomic-bond-relaxation mechanisms. Interestingly, we find the anomalous interfacial adhesion energy and local interface separation are determined not only by the membrane thickness, but also by substrate surface parameters, which suggest that the origin of the topographic fluctuation of graphene on stepped substrates can be attributed to the unique interfacial adhesion behavior.

## Principle

In order to address the influences of surface relaxation and interface mismatch effects as well as the bending of the membrane on the interfacial adhesion properties of graphene, we consider a multilayer graphene with volume $V_0$, area $A_g$, and thickness $t_f$ on a stepped substrate surface, as depicted in Fig. 1. In Fig. 1(b) we show the geometric relationship when a bending graphene is placed at the step edge of the substrate. Naturally, it can be divided into three regions (Fig. 1(b)): I and III stand for the two terraces with different crystallographic orientations, while region II denotes the bending deformation zone. Theoretically, the total free energy of the graphene membranes can be attributed to contributions from the interfacial van der Waals interaction and the elastic strain energy stored in the membrane,

$$U_{\text{total}}^{(hkl)} = U_{\text{vdw}}^{(hkl)} + U_{\text{e}} \quad (1)$$

where $U_{\text{vdw}}^{(hkl)}$ is the interfacial potential energy between the graphene and the substrate in the (*hkl*) crystallographic orientation. $U_{\text{e}} = U_{\text{e}}^{\phi}$ ($\phi$ = I, III) + $U_{\text{e}}^{\text{II}}$ is the total elastic strain energy that includes the summation of deformation strain energy, $U_{\text{e}}^{\text{II}}$, (stored in II zone) and the strain energy, $U_{\text{e}}^{\phi}$ ($\phi$ = I, III), (stored in I and III zones) due to interfacial and surface effects.

In our approach we only consider that the interfacial van der Waals interaction energy is focused on the first layer and the substrate because almost 99% energy is concentrated in this area.[9] Thus, the interfacial potential energy can be written as, $W = \int_{A_g}\int_{V_s} W_{\text{LJ}}\rho_{s,(hkl)}\rho_g \mathrm{d}V_s \mathrm{d}A_g$, where $W_{\text{LJ}} = -C_1/r^6 + C_2/r^{12}$ is the van der Waals interaction between a carbon and a substrate atom, $r$ is the distance between the two atoms, $C_1$ and $C_2$ are the constants related to the material for the attractive and repulsive interactions, $\rho_g$ and $\rho_{s,(hkl)}$ are the number of atoms per unit area of a monolayer graphene and the number of atoms per unit volume of the substrate in the (*hkl*) orientation, $V_s$ is the substrate volume. Consequently, the interfacial potential energy can be obtained,

$$U_{\text{vdw}}^{(hkl)} = -\Gamma_0^{(hkl)}\left[\frac{3}{2}\left(\frac{r_{0,(hkl)}}{r_{(hkl)}}\right)^3 - \frac{1}{2}\left(\frac{r_{0,(hkl)}}{r_{(hkl)}}\right)^9\right] \quad (2)$$

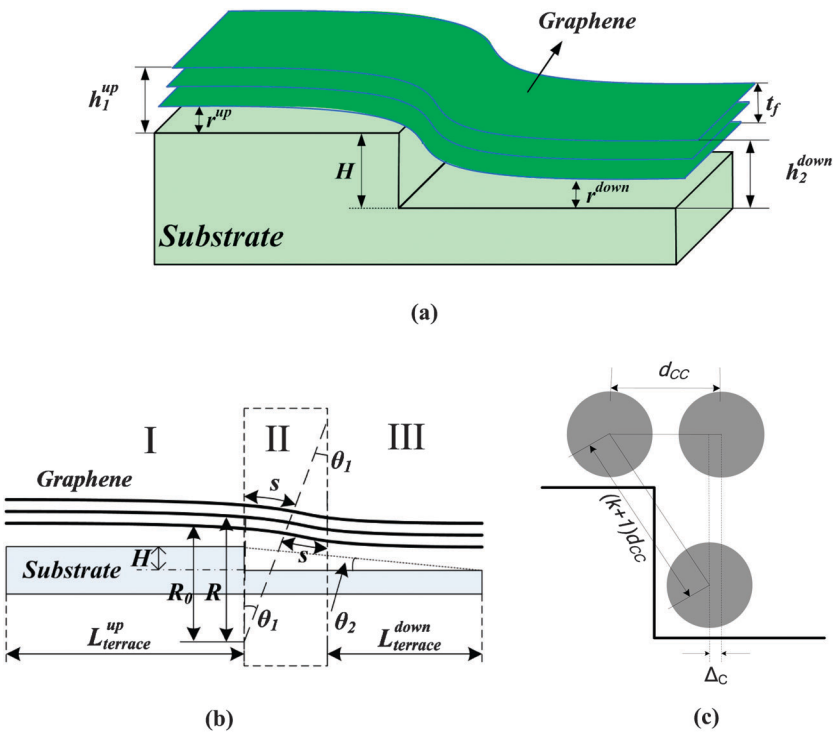


Fig. 1 (a) Schematic illustration showing a multilayer graphene on a stepped substrate surface. $t_f$ is the thickness of graphene membrane, $r^{up}$ and $r^{down}$ are the interface separations between graphene and substrate in up- and down-terrace surfaces, $h_1^{up} = r^{up} + t_f$ and $h_2^{down} = r^{down} + t_f$ represent the heights between the top layer of graphene and the substrate on the two different terrace surfaces. (b) Geometric relationships of the multilayer graphene on the stepped surface. $\theta_1$ and $\theta_2$, respectively, are the central angle due to the bending of graphene and the vicinal angle. The regions I, II and III correspond to the flat and step areas of the substrate. (c) Schematic illustration of a change in position of carbon atoms located at the edge of step.

where $r_{0,(hkl)}$ is the interfacial separation under equilibrium, $\Gamma_0^{(hkl)} = \pi\rho_{s,(hkl)}\rho_g C_1/9r_{0,(hkl)}^3$ is the intrinsic adhesion energy per unit area in $(hkl)$ of the bulk case.[27] In various crystallographic orientations the intrinsic adhesion energy can be calculated as follows,

$$\frac{\Gamma_0^{(h_1k_1l_1)}}{\Gamma_0^{(h_2k_2l_2)}} = \frac{\rho_{s,(h_1k_1l_1)}}{\rho_{s,(h_2k_2l_2)}}\left(\frac{r_{0,(h_2k_2l_2)}}{r_{0,(h_1k_1l_1)}}\right)^3 \quad (3)$$

It is generally known that the performance of surface or edge atoms of nanosolids will dominate due to lower coordination numbers (CNs) and stronger bonds with reduced size.[28,29] In particular, for the coherent bilayer systems consisting of graphene and rough substrate, the mismatch strain and associated with elastic energy will influence the stabilizing graphene and the critical graphene nucleus size.[30] Thus, the bilayer system will be in the self-equilibrium state due to surface and interfacial effects.[10,31,32] Commonly, the interface mismatch strain can be expressed as: $\varepsilon_{int,(hkl)} = (a_{s,(hkl)} - a_f)/a_f$, where $a_f$ and $a_{s,(hkl)}$ are the in-plane lattice constants of graphene and the substrate in $(hkl)$ orientation. In addition, the surface effect of epitaxial layers can be considered by an atomic-bond-relaxation (ABR) method.[29,33,34] Definitely, the key ideal ABR is that the bond loss of an atom in the surface layer will result in the remaining bonds of the less-coordinated atom to shrink spontaneously. As a result, some relevant quantities such as density of charge, mass, and bond energy will be different compared with those of the bulk counterparts and will further impact the Hamiltonian and atomic cohesive energy, *etc.*

In combination with the surface and interfacial effects in graphene on substrate, the total strain in graphene membranes is

$$\varepsilon_f = \frac{\sum_{i<n}\varepsilon_i h_i + \varepsilon_{\parallel,(hkl)}\left(t_f - \sum_{i<n} h_i\right)}{t_f} \quad (4)$$

where $\varepsilon_i = c_i - 1$ is the strain of the $i$th surface atomic layer, $\varepsilon_{\parallel,(hkl)} = \varepsilon_{int,(hkl)}(\varepsilon_{int,(hkl)} + 1)h_0/t_f$ is the strain in the interfacial layers for $(hkl)$ direction, $h_i$ and $h_0$ represent the atomic bond length of the $i$th atomic layers and that of the bulk, $n$ is the number of surface atomic layers, $c_i = 2/(1 + \exp((12 - z_i)/8z_i))$ denotes the CN-dependent bond contraction coefficient with $z_i$ being the effective CNs in the $i$th atomic layer.[35,36] We note that the thickness of multilayer graphene can be expressed as: $t_f = \sum_i c_i h_0$.

In our case we assume the substrate is rigid and the strain energy is primarily focused on the membranes. Therefore, in terms of continuum mechanics, the strain energy (per unit area) for the limiting case of interfacially confined graphene is given by

$$U_e^{\phi}(\phi = I, III) = \frac{Y(t_f)t_f\varepsilon_f^2}{1-\nu} \quad (5)$$

Here $Y(t_f)$ is the thickness-dependent Young's modulus of graphene membranes[34] and $Y(t_f) = Y_B\left\{\frac{z_b}{\langle z\rangle}\left[\sum_{i<n}\gamma_i(z_{ib}c_i^{-m} - 1) + 1\right](1+\varepsilon_f)^{-3}\right\}\cdot z_{ib} = z_i/z_b$ and $\langle z\rangle = \gamma_i(z_i - z_b) + z_b$ are the CN ratios between the $i$th atomic layer and that of the bulk, and the mean CNs, $Y_B$ is the bulk Young's modulus, $m = 2.56$ is an index that characterizes the nature of carbon bonds, $\gamma_i = \sum_{i<n} c_i h_0/t_f$ is the surface-to-volume ratio.

Additionally, we consider a multilayer graphene across the step edge is approximated by two identical arcs of cylinders with radius, $R$, and arc angle, $\theta_1$, of which a schematic illustration is depicted in Fig. 1(b). Note that the curvature of bent graphene is not imposed but is the natural relaxation.[37] According to the theory of elasticity,[38] the moment $M$ of the membrane can be related to the Young's modulus and the curvature $R$, *i.e.*, $M = Y(t_f)I/R$, where $I = L_x t_f^3/12$ is the moment of inertia with $L_x$ being the length of terrace. Thus, the bending strain energy stored in the region II of graphene can be calculated

$$U_e^{II} = 2\int\frac{M^2 ds}{2YI} = \frac{Y(t_f)L_x t_f^2\theta_1}{12}\ln\frac{R_0 + t_f}{R_0} \quad (6)$$

where $R_0$ and $s$ are the radius of the innermost layer of graphene and the arc length of region II depicted in the Fig. 1(b).

Considering the lattice strain induced by surface relaxation and interfacial misfit, as well as the van der Waals interaction between graphene and the substrate, the relationship between the critical interface separation $r_{(hkl)}^*$ in the $(hkl)$ direction and the membrane thickness $t_f$ should be obtained by setting $\partial U_{total}^{(hkl)}/\partial h_{(hkl)} = \partial U_{vdw}^{(hkl)}/\partial r_{(hkl)} + \partial U_e/\partial t_f$. Thus, we have

$$\left(\frac{r_{0,(hkl)}}{r_{(hkl)}^*}\right)^{10} - \left(\frac{r_{0,(hkl)}}{r_{(hkl)}^*}\right)^4 = \frac{2r_{0,(hkl)}\partial U_e}{9\Gamma_0^{(hkl)}\partial t_f} \quad (7)$$

with

$$\frac{\partial U_e}{\partial t_f} = \frac{\sum S_\varphi \partial U_e^\phi/\partial t_f + S_{II}U_e^\phi/R - \partial U_e^{II}/\partial t_f}{\sum S_\varphi} - \frac{\sum\left(S_\varphi U_e^\phi - U_e^{II}\right)S_{II}/R}{\left(\sum S_\varphi\right)^2},$$

$$\frac{\partial U_e^\phi}{\partial t_f} = \frac{t_f\varepsilon_f^2}{1-\nu}\frac{\partial Y(t_f)}{\partial t_f} + \frac{\varepsilon_f^2}{1-\nu}Y(t_f) + \frac{2Y(t_f)(\varepsilon_\parallel - \varepsilon_f)\varepsilon_f}{1-\nu},$$

$$\frac{\partial U_e^{II}}{\partial t_f} = \frac{L_x t_f^2\theta_1}{12}\ln\frac{R_0 + t_f}{R_0}\frac{\partial Y(t_f)}{\partial t_f} + \frac{Y(t_f)L_x t_f\theta_1}{6}\ln\frac{R_0 + t_f}{R_0} + \frac{Y(t_f)L_x t_f^2\theta_1}{12(R_0 + t_f)},$$

and

$$\frac{\partial Y(t_f)}{\partial t_f} = \frac{Y(t_f)}{t_f}\left\{\sum_{i<n}\frac{\gamma_i(z_i - z_b)}{\langle z\rangle} - \frac{1}{1 + \left[\sum_{i<n}\gamma_i(z_{ib}c_i^{-m} - 1)\right]^{-1}} - \frac{3(\varepsilon_\parallel - \varepsilon_f)}{(1+\varepsilon_f)}\right\}$$

where $S_\varphi$ ($\varphi$ = I, II, III) represent the I, II and III regions. It should be noted that $S_{II} = 2R\theta_1 L_x$, where $R = R_0 + t_f/2$ is the radius of middle layer of membrane shown in Fig. 1(c).

 

As a result, by considering the total strain from the surface and interfacial effects as well as the deformation and the van der Waals interactions, the total free energy for graphene on stepped substrate surfaces in a self-equilibrium state can be obtained:

$$\tilde{U} = -\sum \Gamma_0^{(hkl)} \left[ \frac{3}{2}\left(\frac{r_{0,(hkl)}}{r_{(hkl)^*}}\right)^3 - \frac{1}{2}\left(\frac{r_{0,(hkl)}}{r_{(hkl)^*}}\right)^9 \right] - \frac{\frac{Y(t_f)t_f\varepsilon_f^2}{1-\nu}\sum S_\varphi - U_e^{II}}{\sum S_\varphi} \quad (8)$$

## Results and discussion

Hernández *et al.*[39] pointed out that the well-defined parameterization of bulk graphite (*e.g.*, a Young's modulus of 1.02 TPa) cannot be suitable for the case of graphene. In fact, the thickness dependence of the Young's moduli of graphene membranes has been demonstrated both experimentally and theoretically.[40,41] Apparently, the Young's modulus of graphene is an important parameter that determines the interfacial adhesion properties. Therefore, in our case we first calculate the Young's modulus of graphene membranes and the results are shown in Fig. 2. Note that the related parameters used in the calculations are given in Table 1. Clearly, the Young's moduli of graphene membranes from 1–5 layers, respectively, are 3.14, 1.71, 1.41, 1.29 and 1.23 TPa, which increase dramatically with decreasing membrane thickness. The symbols shown in Fig. 2 represent the relevant experimental and theoretical results[40,41] that are in good agreement with our predictions.

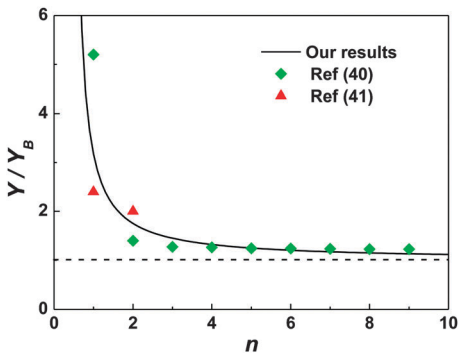


Fig. 2 Young's moduli of graphene membranes. The solid line denotes our predictions, while the symbols represent the available evidences.

Table 1 Input parameters for calculations. $r_0$, $a$, $h_0$, $E$, $\nu$ and $Y_B$ are the interface equilibrium distance, in-plane lattice constant, bond length, binding energy per unit area, Poisson's ratio and Young's modulus, respectively

| | $r_0$ [nm] | $a$ [nm] | $h_0$ [nm] | $E$ [meV Å$^{-2}$] | $\nu$ | $Y_B$ [TPa] |
|---|---|---|---|---|---|---|
| Graphene | 0.34[49] | 0.2445[51] | 0.142[4] | | 0.16[3] | 1.02[49] |
| Cu | | 0.361[43] | | | | |
| $SiO_2$ | | 0.499[52] | | | | |
| Graphene/$SiO_2$ | 0.3[50] | | | 17.01[50] | | |

In nature, the underlying substrate surface parameters, including terrace width and step height, will affect the interfacial adhesion properties of the upper epitaxial layer. In terms of the geometric relationship depicted in Fig. 1(c), the bending of graphene at the step edge necessarily induces a $\Delta_C$ shift in the graphene structure perpendicular to the step edges. There exists a geometric relationship:[17] $H/2 = R(1 - \cos\theta_1)$ and $\Delta_C = 2R\sin\theta_1 - 2R\theta_1 + kd_{CC}$, where $H$ and $d_{CC} = (\sqrt{3}a_f)$ are the step height and the carbon period along the bending direction, $k$ is the integer number of carbon rings that takes the integer part of $H/d_{CC}$, and $k = 0$ if $H \leq d_{CC}$. Therefore, we obtain the relationship as $\sqrt{(k+1)^2 d_{CC}^2 - H^2} - d_{CC} \leq \Delta_C \leq 0$ and further get the average values of $R$ and $\theta_1$. In our calculation we obtain the values of $R$ as 23.3, 35.3, and 72.9 nm when $H$ = 0.5, 0.349 and 0.174 nm, respectively.

Based on eqn (8), the total free energy of graphene placed on $SiO_2$(001) at a fixed terrace width 300 nm and step height 0.5 nm under different vicinal angles $\theta_2$ is calculated and the results are shown in Fig. 3. Strikingly, we find that the minima

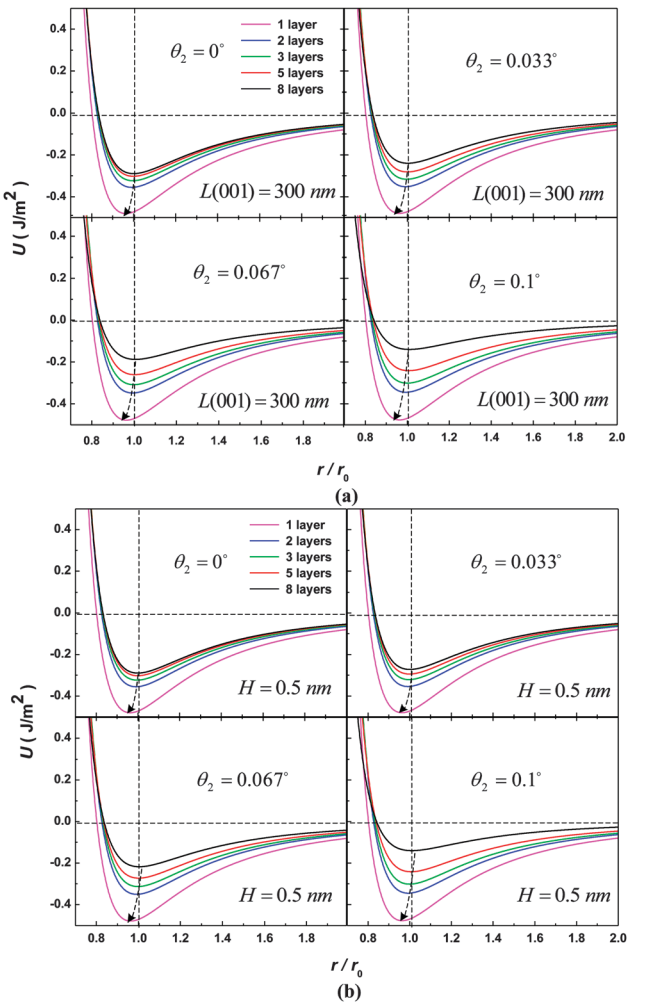


Fig. 3 The relationship between total free energy, number of layers and interfacial separation of graphene/$SiO_2$ under (a) $L$(001) = 300 nm and (b) $H$ = 0.5 nm at fixed vicinal angles, $\theta_2$ = 0°, 0.033°, 0.067° and 0.1°.

of total free energies show an obvious shift with number of layers and this is a function of the substrate surface parameters. Physically, this is attributed to the graphene membrane thickness-dependent Young's modulus that can be modulated by elastic strain energies stored in the membrane.[42]

With the aim of gaining a better understanding of the interfacial separation in graphene/$SiO_2$(001), we extract the critical values from Fig. 3 and re-describe the variant trend as shown in Fig. 4(a). This clearly shows that the interface separation becomes larger with an increasing number of layers and vicinal angles. Interestingly, the interfacial separation became larger than the intrinsic equilibrium distance as the membrane thickness increased. In fact, these results can be attributed to the changes of the geometrical parameters of substrate surface. When the vicinal angle becomes larger, the step height will be higher at fixed terrace width, whereas the terrace width becomes smaller at fixed step height. Both of these two cases lead to the enhancement of the bending elastic energy stored in the membranes and results in the variation of the interfacial separation. Notably, the interaction between graphene and the edge step (vertical to the terrace surface) in II zone can be generally ignored. It is concluded that the contribution of the bending strain energy to the total free energy becomes more pronounced than that of the energy induced by the surface relaxation and interfacial mismatch when both terrace width and step height increase at a fixed vicinal angle. Aitken *et al.*[27] reported that the bending strain energy of graphene has an ineffaceable contribution to the interface separation, and they found the interface separation changes with variation of elastic strain energy, which is consistent with our calculations.

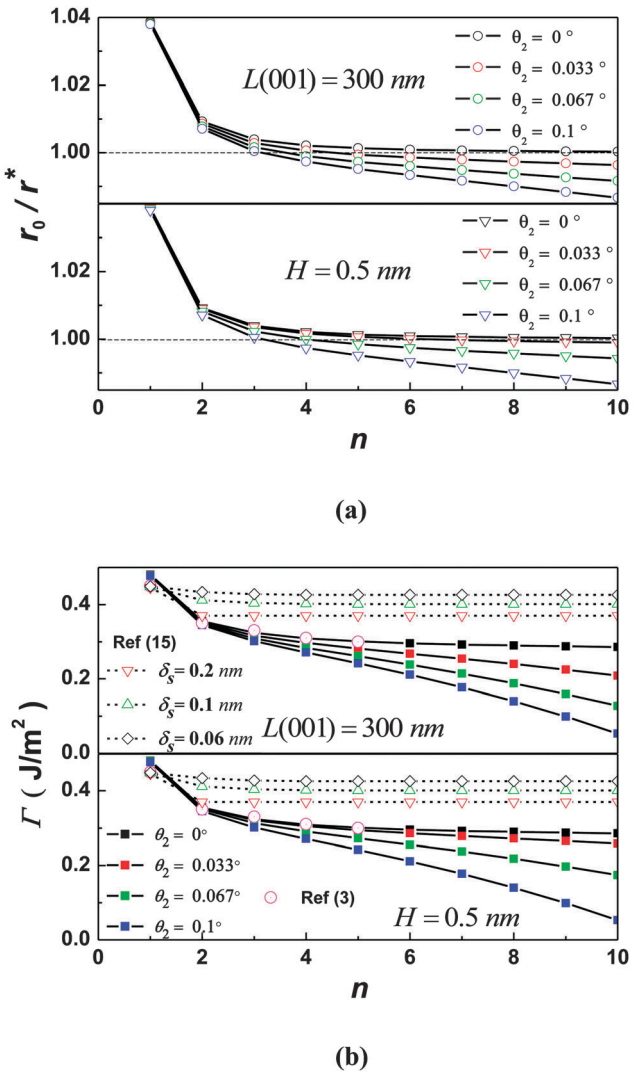


Fig. 4 Dependence of critical interface separation (a) and interfacial adhesion energy (b) on the membrane thickness, vicinal angle and terrace width for graphene/$SiO_2$.

Theoretically, the interfacial adhesion energy is related to the total free energy in the equilibrium state, *i.e.*, $\Gamma = -\tilde{U}$. As illustrated in Fig. 4(b), the interfacial adhesion energy is shown as a function of the number of layers, terrace width, edge height and vicinal angles. Apparently, the interfacial adhesion energy increases with a reduction in membrane thickness, which is in accordance with the experimental observations.[3] Also, the adhesion energy shows a slight change with different vicinal angles from monolayer to trilayer of graphene unless the number of layers reaches or exceeds four. This is mainly because the bending strain energy is much smaller than the surface and interfacial strain energies stored in monolayer to trilayer graphene. When the graphene layers increase, the bending strain energy becomes larger and the surface and interfacial strain energies diminish, thus the adhesion energy will be different with varying vicinal angles. On the other hand, we find the interface adhesion energy decreases with increasing vicinal angles at a fixed terrace width and step height. For example, in the case of bilayer graphene the adhesion energies are, respectively, 0.355, 0.352, 0.349, 0.345 J m$^{-2}$ at a fixed terrace width 300 nm, and 0.355, 0.354, 0.351, 0.345 J m$^{-2}$ at fixed step height 0.5 nm under the condition of vicinal angles ranging from 0° to 0.1°. Gao *et al.*[15] reported that the interfacial adhesion energy would diminish with an enhancement of the roughness of substrate (*e.g.*, a sinusoidal surface with surface amplitude $\delta_s$). Noticeably, the symbols shown in Fig. 4(b) represent the cases from both planar[3] and sinusoidal substrate surfaces.[15] Evidently, the general trends of our predictions agree well with the results of Gao and co-workers.[15] Moreover, in our approach we further consider the surface relaxation and interface mismatch effects and find the interfacial adhesion energy can be tuned by the underlying substrate surface parameters.

In order to further demonstrate the consistency of our analysis, we consider a multilayer graphene placed on Cu(111) with two different stacking modes in up- and down-terrace, as shown in Fig. 5(a). Using eqn (3) and through setting $\Gamma_0^{up}$ = 13.19 meV Å$^{-2}$, $r_0^{up}$ = 0.326 nm,[43] and a fixed interface separation of the down-terrace, $r_0^{down}$ = 0.224 nm, we obtain $\Gamma_0^{down}$ = 18.88 meV Å$^{-2}$, which is very close to the top-hcp structure, 20.2 meV Å$^{-2}$ reported by Xu and Buehler's calculations.[43] Under these circumstances, the critical interface separation and the interface adhesion energy can be calculated by eqn (7) and (8).

 

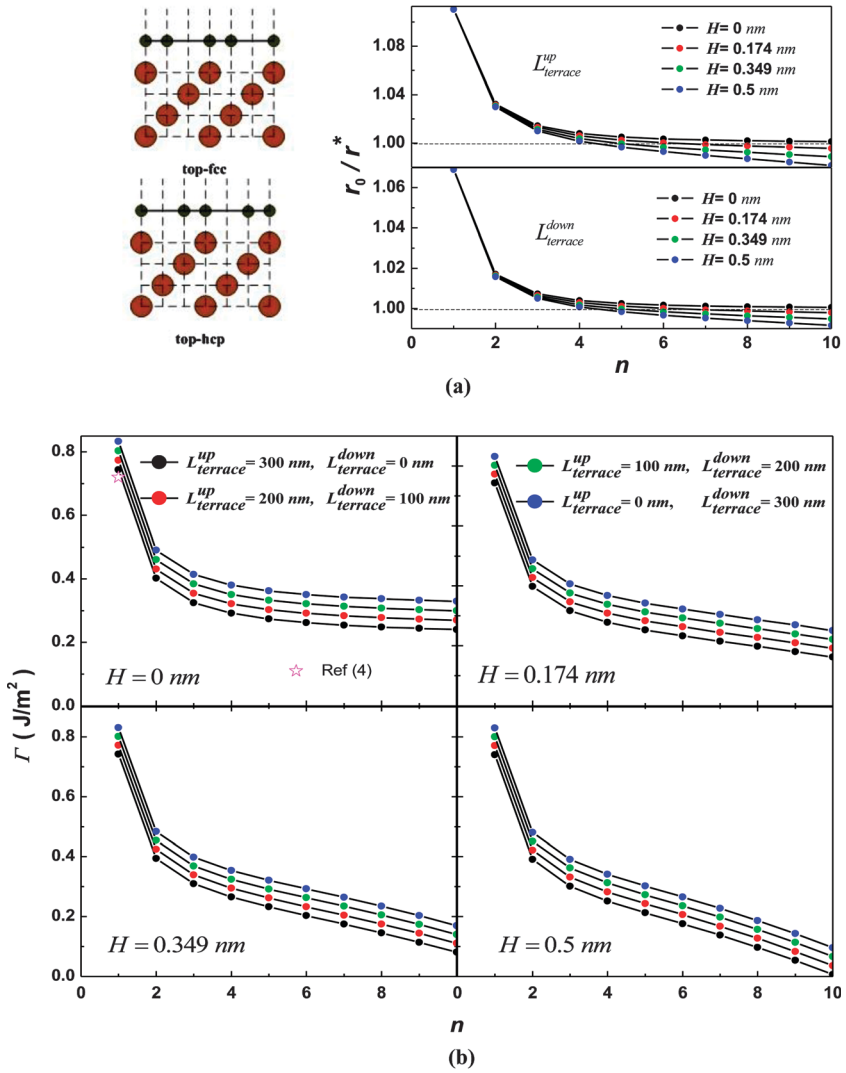


Fig. 5 Dependence of critical interface separation (a) and interfacial adhesion energy (b) on the membrane thickness, vicinal angle, step height, terrace width and crystalline orientation for graphene/Cu. Note that the structures considered for graphene/Cu surface seen from the left side of (a) and the color codes for carbon and copper atoms are black and brown, respectively.

Fig. 5(a) also shows the relationship among critical interface separation, number of graphene layers, different stacking modes in up- and down-terrace and step heights. Clearly, the critical interface separations in both cases increases with rising number of graphene layers, and even beyond the intrinsic interface separation under the flat surface if the underlying substrate surface has existant steps. By contrast, the interfacial separation in up-terrace is larger than that of down-terrace, which is due to various interfacial binding energy and associated with the existing elastic strain energies in two different stacking modes. In addition, from the comparison of the interfacial separation in graphene/Cu and graphene/$SiO_2$, we find the main difference between the two cases: (i) the shift of interfacial separation in graphene/Cu will take place when the membrane thickness is beyond 4 layers, while in graphene/$SiO_2$ the shift is at 3 layers, and (ii) the interfacial separation in graphene/Cu is less than that in graphene/$SiO_2$. This is due to the different mismatches in strain energy, interfacial bonding energy and intrinsic interface separation of the two systems.[44] Moreover, as plotted in Fig. 5(a), when the step height becomes zero, *i.e.* $H$ = 0 nm, the results are consistent with the case of a flat substrate surface.[11]

The corresponding interfacial adhesion energy in graphene/Cu is shown in Fig. 5(b). Similarly, it shows an evident thickness effect and can be determined by the substrate surface parameters such as terrace width and step height. For instance, the adhesion energy increases with diminishing terrace width. Also, the adhesion energy increases with the step height, which is similar to Fig. 4(b). It should be noted that the case is the same as the flat surface when we fixed $H$ = 0 nm, $L^{up}_{terrace}$ = 300 nm, and $L^{down}_{terrace}$ = 0 nm, which agree with the experimental measurements reported by Yoon *et al.*[4] Note that the star symbol shown in Fig. 5(b) indicates the measurable value from Yoon *et al.*[4]

Remarkably, we find that the interfacial adhesion energy is approximately equal to zero when the thickness reaches 10 layers

as plotted in Fig. 5(b), indicating that the graphene will detach from the substrate with an increase of membrane thickness. Thus, the detachment of graphene on a stepped substrate is determined by the underlying substrate surface parameters, including terrace orientation, terrace width and height, *etc.* Scharfenberg *et al.*[14] observed that the graphene undergoes a sharp snap-through transition between conforming to the substrate and lying on top of the substrate with a sinusoidal surface at a critical layers, which implies that the adhesion energy becomes weaker and the graphene can be extracted easily. Besides, Li and co-workers[45–48] found that the detachment of graphene on Si nanosolids (*e.g.*, nanowires and nanoparticles) is determined by interfacial bonding energy, diameter and interspacing between two nanosolids. Therefore, our predictions are in accordance with these evidences, suggesting that the developed method can be an effective tool for tailoring the related mechanical properties of graphene to the desired applications.

## Conclusions and outlook

We establish an analytic method to explore the interfacial adhesion properties in graphene membranes from the perspective of an atomistic origin. As examples we analyzed two types of systems, *i.e.*, graphene/$SiO_2$ and graphene/Cu, and found that the effects of the adhesion energy and local interface separation in a self-equilibrium state depend on the underlying substrate parameters, including step height, vicinal angle, terrace width, and membrane thickness, *etc.* It is demonstrated that the surface relaxation and interface mismatch and associated with elastic strain energy stored in the graphene membranes affect the physical properties such as the Young's modulus and the local interface separation. In addition, we predict an effective way to extract graphene from the underlying substrate through modifying the substrate surface parameters (*e.g.*, steps height, terrace width, and the substrate surface orientation.). Our results agree reasonably well with the theoretical calculations and the experimental measurements. Therefore, we expect that the developed method could be regarded as a theoretical tool to design the interface adhesion of graphene membranes in graphene-based nanomechanical and nanoelectronic devices.

## Acknowledgements

This work was supported by the National Natural Science Foundation of China (Grant No. 11174076 and 91233203), the Hunan Provincial Natural Science Foundation of China (No. 12JJ1009 and 11JJ7001) and Scientific Research Fund of Hunan Provincial Education Department (No. 12A082).

## References

1 A. K. Geim, *Science*, 2009, **324**, 1530.
2 N. A. H. Castno, F. Guinea, N. M. R. Penes, K. S. Novoselov and A. K. Geim, *Rev. Mod. Phys.*, 2009, **81**, 109.
3 S. P. Koenig, N. G. Boddeti, M. L. Dunn and J. S. Bunch, *Nat. Nanotechnol.*, 2011, **6**, 543.
4 T. Yoon, W. C. Shin, T. Y. Kim, J. H. Mun, T. Kim and B. J. Cho, *Nano Lett.*, 2012, **12**, 1448.
5 Y. Ogawa, B. Hu, C. M. Orofeo, M. Tsuji, K. Ikeda, S. Mizuno, H. Hibino and H. Ago, *J. Phys. Chem. Lett.*, 2012, **3**, 219.
6 S. Xia and L. Ponson, *Phys. Rev. Lett.*, 2012, **108**, 196101.
7 S. Das, D. Lahiri, D. Y. Lee, A. Agarwal and W. Choi, *Carbon*, 2013, **59**, 121.
8 T. S. Chow, *Phys. Rev. Lett.*, 2011, **86**, 4592.
9 M. Neek-Amal and F. M. Peeters, *Phys. Rev. B: Condens. Matter Mater. Phys.*, 2012, **85**, 195445.
10 J. Zheng, Y. Wang, L. Wang, R. Quhe, Z. Ni, W. N. Mei, Z. Gao, D. Yu, J. Shi and J. Lu, *Sci. Rep.*, 2013, **3**, 2081.
11 Y. He, W. F. Chen, W. B. Yu, G. Ouyang and G. W. Yang, *Sci. Rep.*, 2013, **3**, 2660.
12 Y. Kim, J. Lee, M. S. Yeom, J. W. Shin, H. Kim, Y. Cui, J. W. Kysar, J. Hone, Y. Jung, S. Jeon and S. M. Han, *Nat. Commun.*, 2013, **4**, 2114.
13 S. Scharfenberg, D. Z. Rocklin, C. Chialvo, R. L. Weaver, P. M. Goldbart and N. Mason, *Appl. Phys. Lett.*, 2011, **98**, 091908.
14 S. Scharfenberg, N. Mansukhani, C. Cesar, R. Weaver and N. Mason, *Appl. Phys. Lett.*, 2012, **100**, 021910.
15 W. Gao and R. Huang, *J. Phys. D: Appl. Phys.*, 2011, **44**, 452001.
16 H. I. Rasool, E. B. Song, M. J. Allen, J. K. Wassei, R. B. Kaner, K. L. Wang, B. H. Weiller and J. K. Gimaewski, *Nano Lett.*, 2011, **11**, 251.
17 J. Coraux, A. T. N'Diaye, C. Busse and T. Michely, *Nano Lett.*, 2008, **8**, 565.
18 Y. F. Zhang, T. Gao, S. B. Xie, B. Y. Dai, L. Fu, Y. B. Gao, Y. B. Chen, M. X. Liu and Z. F. Liu, *Nano Res.*, 2012, **5**, 402.
19 J. F. Gao, J. Yip, J. J. Zhao, B. I. Yakobson and F. Ding, *J. Am. Chem. Soc.*, 2011, **133**, 5009.
20 P. Lauffer, K. V. Emtsev, R. Graupner, T. Seyller and L. Ley, *Phys. Rev. B: Condens. Matter Mater. Phys.*, 2008, **77**, 155426.
21 M. L. Bolen, S. E. Harrison, L. B. Biedermann and M. Capano, *Phys. Rev. B: Condens. Matter Mater. Phys.*, 2009, **80**, 115433.
22 N. Tokuda, M. Murata, D. Hojo and K. Yamabe, *Jpn. J. Appl. Phys.*, 2001, **40**, 4763.
23 D. J. Bottomley, H. Omi, Y. Kobayashi, M. Uemastsu, H. Kageshima and T. Ogino, *Phys. Rev. B: Condens. Matter Mater. Phys.*, 2002, **66**, 035301.
24 V. M. Pereira and N. A. H. Castro, *Phys. Rev. Lett.*, 2009, **103**, 046801.
25 W. G. Cullen, M. Yamamoto, K. M. Burson, J. H. Chen, C. Jang, L. Li, M. S. Fuhrer and E. D. Williams, *Phys. Rev. Lett.*, 2010, **105**, 215504.
26 Q. H. Wang, Z. Jin, K. K. Kim, A. J. Hilmer, G. L. C. Paulus, C. J. Shih, M. H. Ham, J. D. Sanchez-Yamagishi, K. Watanabe, T. Taniguchi, J. Kong, P. J. Jarillo-Herrero and M. S. Strano, *Nat. Chem.*, 2012, **4**, 724.
27 Z. H. Aitken and R. Huang, *J. Appl. Phys.*, 2010, **107**, 123531.
28 G. Ouyang, G. W. Yang and G. H. Zhou, *Nanoscale*, 2012, **4**, 2748.

 

29 C. Q. Sun, *Prog. Mater. Sci.*, 2007, **35**, 1.
30 S. Saadi, F. Abild-Pedersen, S. Helveg, J. Sehested, B. Hinnemann, C. C. Appel and J. K. Nørskov, *J. Phys. Chem. C*, 2010, **114**, 11221.
31 Z. M. Zhu, A. Zhang, Y. He, G. Ouyang and G. W. Yang, *AIP Adv.*, 2012, **2**, 042185.
32 G. Ouyang, C. X. Wang and G. W. Yang, *Chem. Rev.*, 2009, **109**, 4221.
33 A. Zhang, Z. M. Zhu, Y. He and G. Ouyang, *Appl. Phys. Lett.*, 2012, **100**, 171912.
34 G. Ouyang, W. G. Zhu, C. Q. Sun, Z. M. Zhu and S. Z. Liao, *Phys. Chem. Chem. Phys.*, 2010, **12**, 1543.
35 Z. M. Zhu, A. Zhang, G. Ouyang and G. W. Yang, *J. Phys. Chem. C*, 2011, **115**, 6462.
36 X. X. Yang, J. W. Li, Z. F. Zhou, Y. Wang, L. W. Yang, W. T. Zheng and C. Q. Sun, *Nanoscale*, 2012, **4**, 502.
37 I. Nikiforov, D. B. Zhang, R. D. James and T. Dumitrică, *Appl. Phys. Lett.*, 2010, **96**, 123107.
38 G. G. Tibbetts, *J. Cryst. Growth*, 1984, **66**, 632.
39 E. Hernández, C. Goze, P. Bernier and A. Rubio, *Phys. Rev. Lett.*, 1998, **80**, 4502.
40 D. B. Zhang, E. Akatyeva and T. Dumitrică, *Phys. Rev. Lett.*, 2011, **106**, 255503.
41 J. U. Lee, D. Yoon and H. Cheong, *Nano Lett.*, 2012, **12**, 4444.
42 M. Poot and H. S. J. van der Zant, *Appl. Phys. Lett.*, 2008, **92**, 063111.
43 Z. Xu and M. J. Buehler, *J. Phys.: Condens. Matter*, 2010, **22**, 485301.
44 L. Y. Jiang, Y. Huang, H. Jiang, G. Ravichandran, H. Gao, K. C. Hwang and B. Liu, *J. Mech. Phys. Solids*, 2006, **54**, 2436.
45 T. Li and Z. Zhang, *Nanoscale Res. Lett.*, 2010, **5**, 169.
46 Z. Zhang and T. Li, *J. Appl. Phys.*, 2010, **107**, 103519.
47 T. Li, *Modell. Simul. Mater. Sci. Eng.*, 2011, **19**, 054005.
48 S. Z. Zhu and T. Li, *J. Appl. Mech.*, 2014, **81**, 061008.
49 C. Lee, X. Wei, J. W. Kysar and J. Hone, *Science*, 2008, **321**, 385.
50 M. Z. Hossain, *Appl. Phys. Lett.*, 2009, **95**, 143125.
51 G. Giovannetti, P. A. Khomyakov, G. Brocks, V. M. Karpan, J. van den Brink and P. J. Kelly, *Phys. Rev. Lett.*, 2008, **101**, 026803.
52 V. Dmitriev, V. Torgashev, P. Toledano and E. K. H. Salje, *Europhys. Lett.*, 1997, **37**, 553.